Pergamon

Int. J. Heat Mass Transfer. Vol. 39, No. 5, pp. 1093–1101, 1996

0017-9310/96 $15.00+0.00

0017-9310(95)00190-5

Local convective mass transfer on circular cylinder with transverse annular fins in crossflow

HYUNG JIN SUNG, JUNG SEUNG YANG and TAE SEON PARK

Department of Mechanical Engineering, Korea Advanced Institute of Science and Technology, 373-1 Kusung-dong Yusong-ku, Taejon, 305-701, Korea

(*Received* 16 *June* 1994 *and in final form* 23 *March* 1995)

Abstract—An experimental study was made of local mass transfer from a circular cylinder, which is situated between two annular fins in a crossflow. Low turbulence-intensity wind tunnel experiments were conducted over moderate Reynolds numbers, $33\,000 < Re_d < 80\,000$. Velocity measurements were analyzed to examine the characteristics of the boundary layer, which is developed on the flat annular fin. The naphthalene sublimation technique was employed to measure the local convective mass transfer around the circular cylinder. The ratio of the axial gap distance between two axial fins (L) to the radial protrusion length of the annular fin (H) was an important experimental parameter, and its range was $0 < L/H < 0.40$. The impact of horseshoe vortices on local mass transfer was scrutinized. For a small gap distance ($L/H = 0.05$), naphthalene sublimation is intense in the front portion of the cylinder, especially near the separation region. When the gap distance is moderate ($L/H = 0.15$), the overall character of sublimation shows a more organized pattern. The influence of horseshoe vortices is substantial. For a large gap distance ($L/H = 0.40$), a dominant role of horseshoe vortices near the corner junction is discernible.

1. INTRODUCTION

Transverse annular-finned tubes are widely used as a means of enhancing convective heat transfer in a crossflow [1]. Narrowly-spaced annular fins of finite length are appendages attached to the base structure. A circular cylinder is a typical such base structure, which aims to extend and expose a broader surface to convection.

The flow around an annular-finned circular cylinder in a crossflow, despite its relatively simple geometry, exhibits extremely complex three-dimensional flow characteristics. Among others, the separated flow, which subsequently reattaches in the downstream locations, is believed to lead to unfavorable flow structures. Also, flow separation increases heat and mass transfer, and fluid mixing intensities. In particular, complex flow patterns caused by the horseshoe vortices at the corner junction are of interest to the study of local heat transfer enhancement mechanism [2–5].

The horseshoe vortex is known to form owing to the adverse pressure gradient near the intersection of two bodies. The mean shear within the approaching boundary layer is skewed, or deflected by the transverse pressure gradient. Accordingly, the boundary layer separates and rolls up to form a spanwise vortex at the leading edge. The horseshoe vortex alters the turbulence structures within the boundary layer, which has serious influences on the overall convective heat transfer. Figure 1 shows a schematic drawing of horseshoe vortex system with several associated smaller vortices, which are abbreviated as $V1$, $V2$ and $V3$. When the gap distance between two annular fins is relatively large, the flow pattern about the circular cylinder may be assumed to be two-dimensional, at least in the central region [6, 7]. When the gap distance becomes narrow, however, the flow pattern between annular fins is fully three-dimensional. The main vortex $V1$ is dominant over the secondary vortex $V2$. $V2$ is generated due to the secondary flow in the vicinity of the junction. The size of the $V2$ vortex is very small, and accurate measurements are called for to identify such small vortices. Furthermore, Goldstein and Karni [8] found an even smaller vortex $V3$, which is formed around the front portion of the cylinder above $V2$.

A literature survey reveals that the general conceptual picture of the horseshoe vortex system has been established by many experimental researchers [6–15]. Among others, Goldstein and Karni [8] measured the local mass transfer near the base of a circular

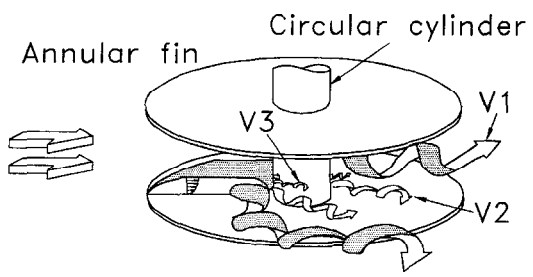

Fig. 1. Schematic flow patterns of horseshoe vortices around the circular cylinder between annular fins.

NOMENCLATURE

d	cylinder diameter
D_f	mass diffusive coefficient for naphthalene vapor in air
h_m	local mass transfer coefficient
H	height of annular fin from the cylinder surface
L	distance between the annular fins
Re_d	Reynolds number based on d, Ud/v
Re_L	Reynolds number based on L, UL/v
Sh	Sherwood number, $h_m d/D_f$
T	temperature
Δt	change in local naphthalene thickness due to sublimation
U	freestream velocity
V	vortices
z	direction along the cylinder between annular fins.

Greek symbols

δ	boundary layer thickness along the annular fin, which is developed from the leading-edge of annular fin
δ^*	displacement thickness of corresponding boundary layer
θ	circumferential angle around the circular cylinder measured from the front stagnation point
$\Delta\tau$	exposure time in wind tunnel
$\rho_{v,w}$	local naphthalene vapor density at wall
ρ_s	density of solid naphthalene.

cylinder placed normal to a flat plate wall boundary layer. It was found that mass transfer was augmented on the cylinder near the junction. This may be attributed mainly to the existence of small, intense secondary vortices within the horseshoe vortex system. Especially, a significant enhancement of mass transfer, attributable to the influence of $V2$ vortex, was observed. The mass transfer rate in the immediate vicinity of the wall is nearly seven times greater than the value in the region far away from the junction. Similar experiments were performed by Van Dresar and Mayle [12] for the base of a circular cylinder (15.2 cm diameter) placed normal to a long splitter plate (96 cm long). The spanwise variation in mass transfer due to the horseshoe vortices was measured. It was shown that the mass transfer rate is a function of δ/d, which indicates the ratio of the boundary layer thickness (δ) to the diameter of circular cylinder (d). However, the effect on the overall mass transfer was seen to be small unless the ratio of the span of the cylinder to the incident boundary layer is of order unity. Previous investigations disclosed that the size, number and positions of the vortices in the separated region in front of the obstacle depend on the approaching boundary layer characteristics, the Reynolds number and the obstacle geometry [12–15].

The main objective of the present study is to explore the local mass transfer around and along a circular cylinder in a crossflow, where narrowly-spaced annular fins of finite size are attached to the cylinder. Emphasis is placed on delineating the horseshoe vortices near the corner junction over the range, $33\,000 < Re_d < 80\,000$. In particular, the study is focused on the circumferential variations of the Sherwood number, Sh. Since two approaching boundary layers are developed concurrently from the leading-edge of the annular fins, a complex flow pattern is induced inside the annular fins. The gap distance between two annular fins is a crucial parameter (Fig. 2). In an effort to understand the correlation between horseshoe vortices and approaching boundary layer characteristics, flow fields along the annular fin are measured. The effect of horseshoe vortices ($V1$, $V2$ and $V3$) on the local mass transfer rate around and along the circular cylinder is investigated by employing the naphthalene sublimation technique. It is known that the naphthalene sublimation technique is adaptable to the precise measurement of local transfer rates in regions with large gradient of transport. This technique has been successfully utilized in various types of mass transfer studies [6–8, 12, 16, 17], and it proves to be a viable experimental tool for the present problem.

2. EXPERIMENTAL APPARATUS AND PROCEDURE

Experiments were performed in an open blower-type wind tunnel. The air speed at the test section (500×500 mm) was varied from 9.3 to 30.0 m s^{-1}, and the free-stream turbulence intensity in the test section was less than 0.2%. No significant peaks were observed in the spectrum of the velocity fluctuations of the main flow.

The diameter of the cylinder was 48 mm and the test cylinder was extended through both side walls of the test section. The channel blockage factor and the

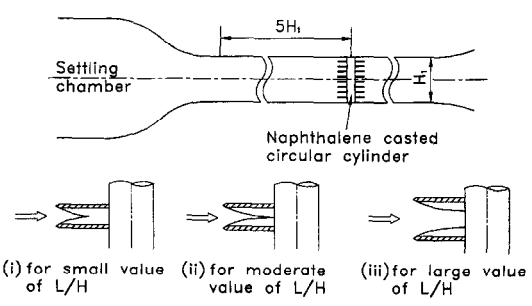

Fig. 2. Schematic view of the wind tunnel and three models of the boundary layer development.

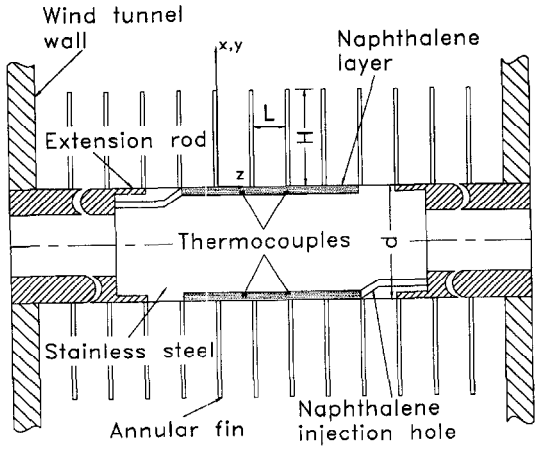

Fig. 3. Naphthalene-cast cylinder with annular fins.

aspect ratio of the cylinder were 0.096 and 10.4 : 1, respectively, which lie within the range of the two-dimensionality assumption [17]. The cylinder consists of two supporting parts and a removable central test section. The total length of the central section was 800 mm, and the portion of the round naphthalene band cast was 48 mm. Figure 3 shows a schematic view of the naphthalene-cast cylinder and the definitions of relevant symbols. In this figure, L denotes the gap distance between annular fins and H is the height of annular fin from the cylinder surface ($H = 96$ mm). A large number of dummy annular fins are attached to the cylinder in the test section so that the flow can be uniformly distributed through the annular fins regardless of L/H. A prototypical picture displaying the annular fins ($L/H = 0.40$) is shown in Fig. 4. The naphthalene-cast section is fabricated, such that a gap distance of desired length could be obtained with relative ease.

Care was exercised in dealing with the naphthalene sublimation technique, which formed the heart of the present experiments. Two pieces of copper mold were specially fabricated, each of which was 80 mm long and 25 mm thick. The test cylinder was precision-mounted inside the mold, and the molten naphthalene was poured into the bottom side of two injection holes. In order to separate the mold from the naphthalene coated cylinder without damaging the surfaces, the difference of the thermal expansion rates between the copper mold and the naphthalene layer was calculated. Six thermocouples were embedded inside the coated cylinder to measure the temperature during the test run, and the time-averaged wall temperature was used to determine the effective vapor concentration [6, 7].

In order to avoid errors caused by extraneous naphthalene sublimation during a lengthy measurement period, a computer-controlled, automated data acquisition system has been designed. It consists of a depth gauge along with a signal conditioner, a digital voltmeter (HP3456a) connected with a GPIB interface, a positioning apparatus driven by three stepper motors, a motor controller, and an IBM-486 personal computer for data storage and reduction. The accuracy of the measurement of the local sublimating mass transfer depends largely on the positioning accuracy. The specially-designed positioning apparatus is shown in Fig. 5, which includes a linear-axis table (LM guide), a rotary table, and a timing belt driven by a stepper motor. The depth gauge (LVDT; linear-variable-differential-transformer) has a spherical contact point with a diameter of 1.2 mm. It is mounted on the guide

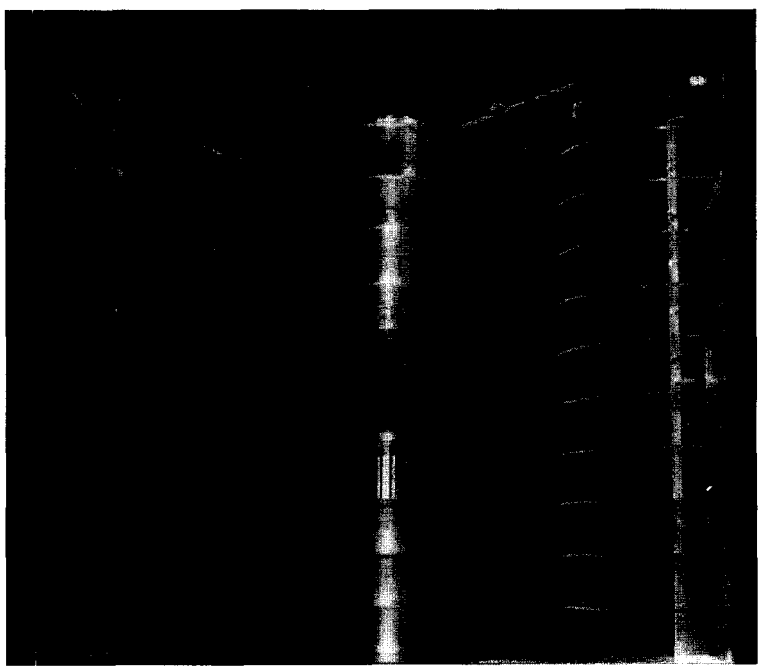

Fig. 4. Exemplary picture of the test section ($L/H = 0.40$).

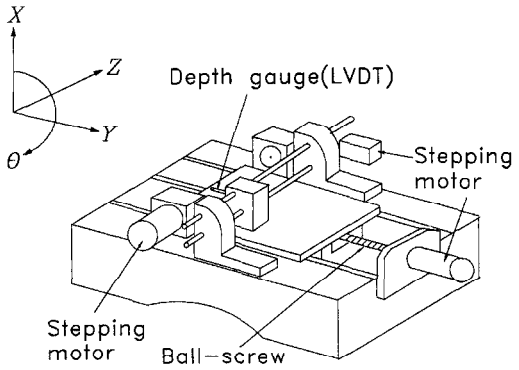

Fig. 5. Schematic model of the positioning apparatus.

block and it can be moved along the cylinder, while the rotary table rotates the cylinder with the desired angle increment by the stepper motor. Each motor step increment moves the depth gauge by 0.0202 mm (i.e. $4.21 \times 10^{-4}d$) or rotates the cylinder by 0.18°.

The repositioning of the cylinder was allowed such that repetitive readings can be taken at the same locations on the surface. For this purpose, a conical shaped recess was indented in the stainless steel surface near the bottom of the cylinder. When the cylinder was installed in the wind tunnel, the recess about 2 mm deep was positioned at a known angle relative to the front stagnation point. Measurements were taken in the following manner. First, the starting point was located in the center of the small recess. Next, the depth gauge was driven along the cylinder, stopping at a designated measurement location. Before each reading was taken, the gauge was given a one-half second stabilization period. Subsequently, the digital voltmeter was triggered and the voltage output of the conditioner of the gauge was transferred to the HP3456a and IBM-486 personal computer for data reduction. The surface profile measurement was conducted at a constant room temperature to avoid errors caused by natural convection during a measurement.

The mass transfer coefficient can be determined from the relation

$$h_m = (\rho_s \Delta t/\Delta\tau)/\rho_{v,w} \quad (1)$$

where ρ_s and $\rho_{v,w}$ denote the density of naphthalene ($\rho_s = 0.975$ kg m^{-3} at 25°C) and the naphthalene vapor concentration at the wall [6, 7]. Here, Δt is the naphthalene thickness sublimated in time $\Delta\tau$. The averaged sublimated thickness during the experiment is typically less than $0.1 \sim 0.2$ mm, which is small enough not to alter seriously the flow field due to the resulting wavy wall. The empirical equation of Ambrose *et al.* [18] is used to determine the naphthalene vapor pressure. From the ideal gas law, naphthalene vapor density on the surface is then evaluated. Explicit details, including the relationship between $\rho_{v,w}$ and the local temperature T, are available (e.g. Sung *et al.* [6]). The results are expressed in terms of the Sherwood number,

$$Sh = h_m d/D_f \quad (2)$$

where the mass diffusion coefficient of naphthalene in air (D_f) is determined from the Mack's measurement data and Chen and Othmer's correlation [19].

The experimental uncertainties associated with the present measurement of h_m are appraised following the procedure of Sung *et al.* [6, 7]. Possible elemental sources of the present experiments may stem from the estimations of the material properties (about 4.4%) and the measurement error. The measurement error is mainly due to the resolution limitation of the positioning apparatus, which is about 5% of the total sublimation depth for an exposure time of about 100 min. This yields the uncertainty in h_m of about 9.4%. Therefore, the experimental uncertainty in the final evaluation of h_m is approximately 10%, which is comparable to other experiments [8, 12].

3. RESULTS AND DISCUSSION

Before commencing the experiment with annular fins, the distribution of local mass transfer around the circular cylinder without annular fins is exhibited in Fig. 6 to ascertain the reliability and accuracy of the present experiment. In accordance with the theoretical prediction by Frössling [8], the ordinate is shown in $Sh/Re_d^{1/2}$ and the abscissa is represented in the circumferential angle θ. As is evident in Fig. 6, the present experiment shows consistency with the relevant data in the upstream regions before separation. The local rate of mass transfer around the circular cylinder is shown to be nearly symmetric. Near the separation region ($\theta = 80°$), mass transfer reaches a minimum. After passing the separation region, Sh gradually increases in the rear portions of the cylinder [21].

In order to investigate the effect of annular fins, three values of L/H, i.e., $L/H = 0.05$, 0.15 and 0.40 are chosen, where L/H denotes the ratio of the gap distance (L) between annular fins to the radial protrusion height (H) of an annular fin. It is known that the mass transfer rate around a circular cylinder depends strongly on the boundary layer thickness along the wall due to the endwall effect [8, 12, 13]. Preliminary measurements of velocity profiles

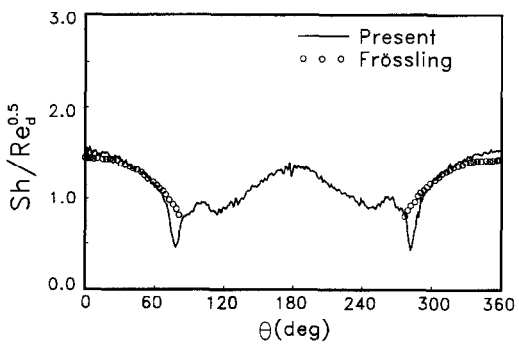

Fig. 6. Circumferential distribution of $Sh/Re_d^{1/2}$ around the cylinder of no fins.

Table 1. Measurement of δ/d at $x/H = 0.5$

	Re_d		
L/H	33 000	66 000	80 000
0.05	—	—	—
0.15	7.81×10^{-2}	6.90×10^{-2}	6.50×10^{-2}
0.40	9.94×10^{-2}	8.73×10^{-2}	8.44×10^{-2}

between the annular fins were conducted to examine the major features of the boundary layer along annular fin-wall. For example, the thickness of the mainstream boundary layer δ at $X/H = 0.5$ is $\delta = 4.19$ mm for $L/H = 0.40$ and $Re_d = 66\,000$, which corresponds to $\delta/d = 8.73\times10^{-2}$ and $\delta/L = 1.09\times10^{-1}$. The characters of the boundary layer during the test runs are summarized in Table 1. As sketched in Fig. 2, a pair of boundary layers develop simultaneously from the edge of the annular fins. Here, the annular fins are placed parallel to the direction of the approach flow. Depending on the values of L/H, qualitatively different flow modes are evident. For a small value of L/H, two boundary layers grow to touch with each other. Thus, the penetration of the main flow is not sufficiently long enough to reach the cylinder surface. For a moderate value of L/H, two layers are merged just in front of the cylinder surface. As L/H increases, however, two boundary layers develop separately.

Now, the mass transfer properties for three values of L/H, i.e. $L/H = 0.05$, 0.15 and 0.40 are scrutinized in Fig. 7. The measurement was performed on the centerplane between the annular fins as a function of θ. The solid line represents the distribution of local mass transfer without annular fins. For a small gap distance ($L/H = 0.05$), it is seen that the mass transfer at the front stagnation region is vigorous. This implies that the active mass transfer due to augmented flow speed in the narrow gap takes place by the presence of annular fins. On the contrary, the mass transfer in the rear side is weak, and this value is even smaller than the mass transfer without annular fins. This is attributed to the fact that the flow resistance between the annular fins increases due to the narrow gap. Thus, the main stream could not penetrate into the cylinder surface. This interpretation is in line with the observation that the minimum value of Sh is moved slightly toward the front stagnation point ($\theta = 75°$).

As the gap distance is moderate ($L/H = 0.15$), the mass transfer rates gradually increase in the rear wake region, which is exhibited in Fig. 7b. Due to the merging of two boundary layers inside the annular fins (Fig. 2b), a secondary flow created by vortices is generated around the cylinder, which, in turn, gives rise to enhanced mass transfer rates. As a result, the minimum point of Sh is pushed backward ($\theta = 84°$).

Figure 7c shows the distribution of $Sh/Re_d^{1/2}$ for $L/H = 0.40$, where the gap distance is fairly wide. For this run, as compared with the case without annular fins, no significant difference is observed in the flow pattern prior to the separation. However, active mass transfer is noted after separation, near the rear-side of the cylinder. Here, the separation point corresponds to the point of minimum Sherwood number. A precise inspection of the distributions indicates that, although two minimum points in $Sh/Re_d^{1/2}$ are observed for $L/H = 0.05$ and 0.15, only one minimum is seen for $L/H = 0.40$.

The effect of L/H on the averaged circumferential mass transfer ($\overline{Sh_\theta}$) in the centerplane between the annular fins is described in Fig. 8. The averaged value ($\overline{Sh_\theta}$) can be obtained from the local mass transfer measurements,

$$\overline{Sh_\theta} = \frac{1}{2\pi}\sum_{j=1}^{n} Sh_j \Delta\theta_j \tag{3}$$

where n is the total number of measurements on the centerplane between the annular fins and $\Delta\theta_j$ denotes the angle increment around the cylinder. For three cases ($Re_d = 33\,000$, 66 000, 80 000), the maximum of

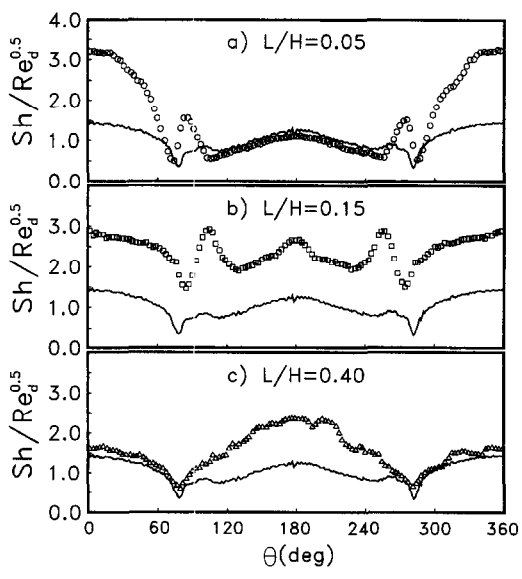

Fig. 7. Circumferential distributions of $Sh/Re_d^{1/2}$ on the centerplane between annular fins. (a) $L/H = 0.05$, (b) $L/H = 0.15$, (c) $L/H = 0.40$.

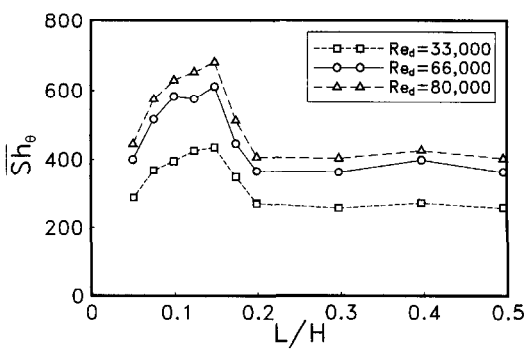

Fig. 8. Distribution of $\overline{Sh_\theta}$ as a function of L/H for $Re_d =$ 33 000, 66 000 and 80 000.

$\overline{Sh_\theta}$ is clearly discernible near $L/H = 0.15$ in Fig. 8, which is almost twice larger than the case without annular fins. This optimal gap distance is a useful value in searching for an enhancement of mass transfer from the cylinder with annular fins. However, it should be emphasized here that the mass transfer from the surface of the annular fin itself is not considered in the present study.

One major aim of the present study is to explore the salient vortex characteristics near the corner junction by utilizing the mass transfer data. It is well known that the boundary layer flow approaching an obstacle undergoes three dimensional separation, and that the separated boundary layer rolls up to form a horseshoe vortex system. Multiple vortices in the vicinity of the endwall, as sketched in Fig. 1, appear to affect the mass transfer significantly [8, 9, 16, 17]. The size of the primary horseshoe vortex $V1$ might be expected to be of the same order of magnitude as the freestream boundary layer thickness. The other vortices are an order of magnitude smaller than $V1$. Some researchers found or proposed a corner vortex $V2$, tucked in the wall-cylinder corner. Goldstein and Karni [8] inferred at least one vortex ($V3$) between the primary vortex and corner vortex in interpretating their mass transfer data on a circular cylinder near the endwall. Considering the rotation direction and mass transfer results, the assumption of a counterrotating vortex ($V3$) seems to be reasonable.

The overall features of mass transfer are visualized in Fig. 9 by means of plots of Sh on the cylinder surface. The corresponding contour plots are also illustrated. The contour lines, which are calculated directly from the measurements, correspond to the pattern of a horseshoe vortex flow as described previously by Goldstein and Karni [8]. A closer inspection of the contour plots reveals that, for a small gap distance ($L/H = 0.05$), the bulk of sublimation takes place near the front region of the cylinder, especially around the separation region. The endwall effect created by the corner vortex is not substantial. When the gap distance is moderate ($L/H = 0.15$), however, the global character of sublimation shows a more organized pattern, i.e. the influence of horseshoe vortices near the endwall is comparable to the effect of vortices near the separation region. The higher peak, which corresponds to $V2$, is located about ($z/d = 0.01$ or $z/L = 0.03$). For a large gap distance ($L/H = 0.40$), the effect of horseshoe vortices on the corner junction in the vicinity of the endwall is dominant. In the interior, the flow is seen to be nearly two-dimensional.

To seek a better understanding of the impact of horseshoe vortices on local mass transfer, the variations of $Sh/Re_d^{1/2}$ on the endwall near the cylinder ($z/d = 0.01$ or $z/L = 0.03$) are shown in Fig. 10. As shown, the sharp increases very near the endwall ($z/d = 0.01$) are caused by the corner vortex $V2$. This vortex is so intense that it creates an observable trench in the naphthalene surface during a test run. As sketched in the schematic flow patterns of vortices in Fig. 1, the swirling corner vortex is directly responsible for intensified mass transfer. For example, the vortex $V2$, which is located very close to the fin-wall, moves along the cylinder with a particular period. As a result, it produces a wavy pattern on the surface due to the corresponding local sublimation. These phenomena are represented in the plot of $Sh/Re_d^{1/2}$ in Fig. 10a. The effect of vortex $V2$ is clearly discernible very close to the fin-wall ($z/d = 0.01$). As can be seen in Fig. 10a, the influence of $V2$ on Sh for $L/H = 0.05$ is not substantial, but the effect of $V2$ for $L/H = 0.15$ is significant. As L/H increases ($L/H = 0.40$), the influence of $V2$ is pronounced near the stagnation region rather than in the wake region. This is consistent with the prior experimental results [8, 12], in which the cylinder was protruded from the boundary layer endwall.

The distributions of $Sh/Re_d^{1/2}$ at a location slightly away from the fin-wall ($z/d = 0.03$) are displayed in Fig. 10b. As compared with the prior measurements ($z/d = 0.01$), the vortex $V2$ patterns are not clearly captured. This implies that, as the location moves away from the wall, the strengths of $V2$ decay considerably, i.e. the effect of vortex $V2$ is concentrated very close to the endwall [8]. As L/H increases, the dominant impact of vortex $V2$ moves toward the rear-side wake region, whereas no significant variations are seen in the stagnation region.

In order to observe the influence of vortex $V3$ on mass transfer, the variations of Sh along the cylinder (z/L) are exhibited in Fig. 11. In this case, some representative circumferential angles are selected to examine their prominent features. Plottings are made for three cases of L/H and the case of no fins. It is generally known that $V3$ is located above $V2$ [8]. A closer inspection of the trajectories of Sh for $L/H = 0.40$ discloses that the second peak of Sh ($V3$) is clearly discernible after the first peak ($V2$) in the circumferential direction, i.e. $\theta = 0°$, $50°$ and $70°$. As θ increases ($\theta = 90°$, $110°$ and $180°$), no peak values caused by $V3$ are seen. For the case of $L/H = 0.40$ and $\theta = 50°$, the vortex $V2$ takes place at $z/L = 0.025$ and the vortex $V3$ occurs at $z/L = 0.05$. In this case, $z/L = 0.025$ corresponds to $z/d = 0.02$. As θ increases, the vortex $V3$ becomes stronger in the region between the stagnation point ($\theta = 0°$) and the separation point, whereas the strength of vortex $V2$ is gradually attenuated. The vortex $V3$ diminishes rapidly after the separation point.

For a moderate value, $L/H = 0.15$, the strength of vortex $V2$ is relatively weak in the front region of the cylinder. The vortex $V3$ is also less distinct, e.g. $\theta = 50°$ and $70°$. A large value of mass transfer is found in the rear parts of the cylinder ($z/L = 0.2$ and $\theta = 110°$). However, for $L/H = 0.05$, a small enhancement of the mass transfer due to the vortex $V3$ is observed. Furthermore, the overall mass transfer is very small, and this value is even smaller than that of the case of no fins.

Figure 12 exhibits the plots of the angles of the minimum value of Sh on the centerplane (Fig. 7). In

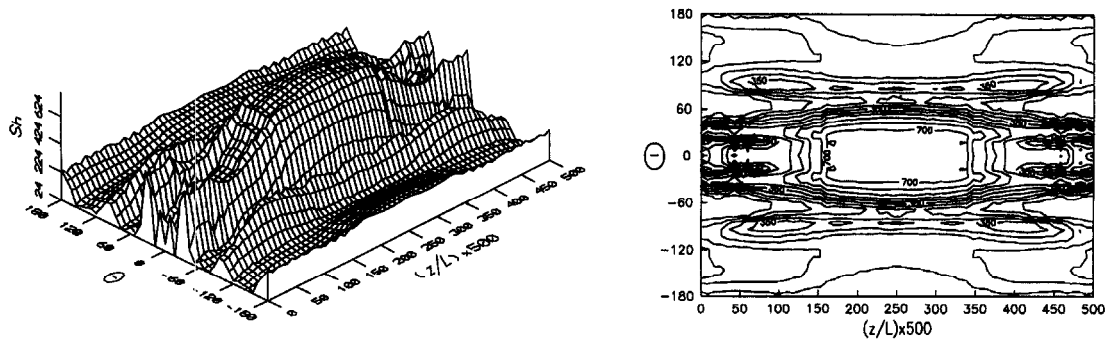

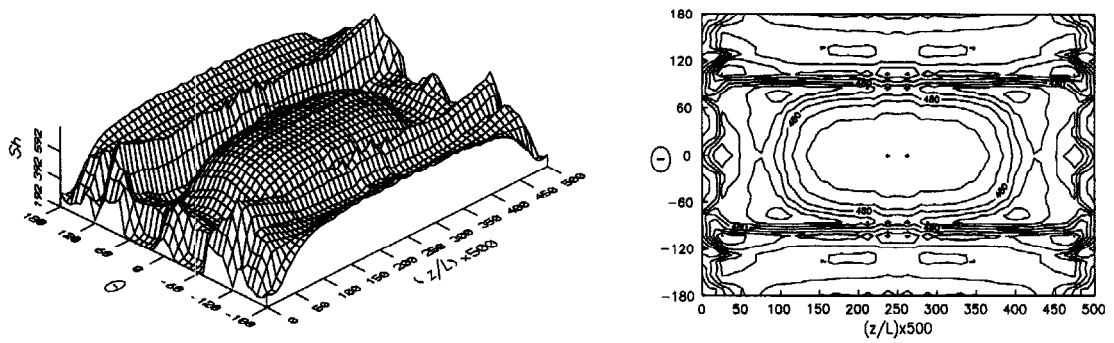

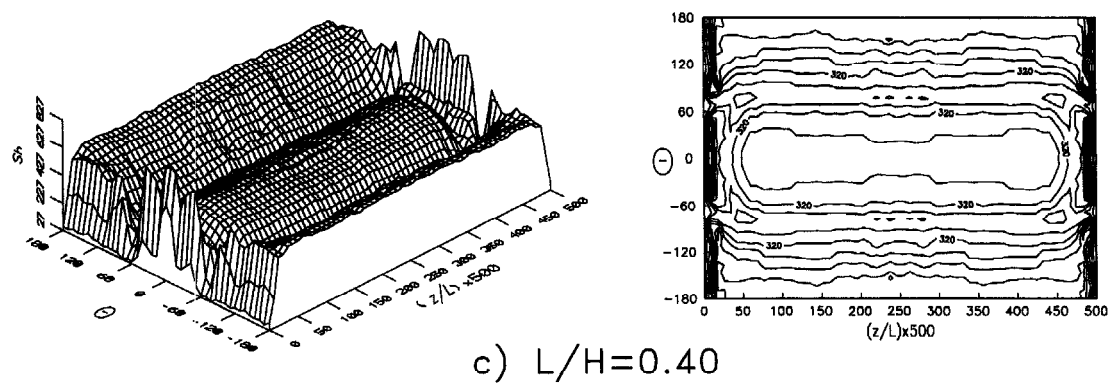

Fig. 9. Surface and contour plots of Sh on the cylinder surface for $L/H = 0.05$, 0.15 and 0.40.

addition, the angles at which the second peak of Sh disappears are also displayed, which can be obtained from Fig. 11. These two angles are plotted against the gap distance (L/H). It is interesting to note that the two curves show similar trends. A rapid decrease of θ at $L/H = 0.15$ is seen for both cases. It means that this value denotes the critical gap distance to characterize the mass transfer. As L/H increases, the two curves gradually converge to their own asymptotic values. In the range $0.075 \leqslant L/H \leqslant 0.15$, it is seen that the angle of the minimum Sh or the angle at which the second peak of Sh disappears maintains the constant value, i.e. $\theta \cong 92°$.

For varying values of L/H, the distributions of the circumferentially-averaged Sherwood number ($\overline{Sh_\theta}$), which is defined in equation (3), are displayed in Fig. 13. For a large gap distance ($L/H = 0.40$), the first maximum of $\overline{Sh_\theta}$ is clearly seen at $z/L = 0.0125$ (i.e. $z/d = 0.01$), which is due to $V2$. For $L/H = 0.05$, however, the influence of $V2$ is negligible. Furthermore, the averaged Sherwood number close to the junction is smaller than that of no fins until $z/L = 0.2$.

4. CONCLUSION

Detailed measurements of local mass transfer from a cylinder between annular fins were obtained by exploiting the naphthalene sublimation technique. The measurement results disclosed the prominent features of horseshoe vortices near the corner junction.

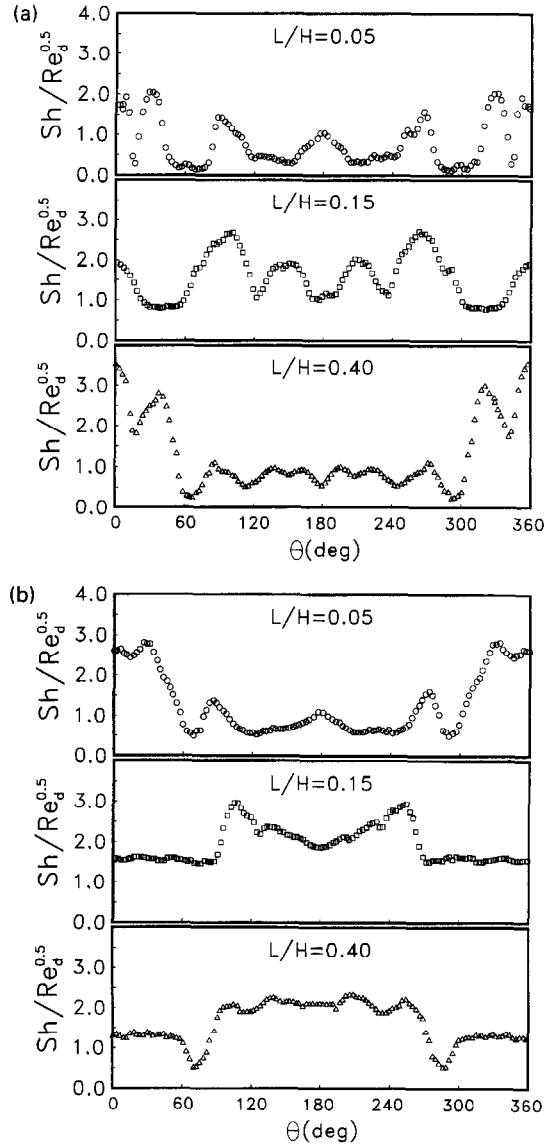

Fig. 10. (a) Circumferential distributions of $Sh/Re_d^{1/2}$ for $z/d = 0.01$. (b) Circumferential distributions of $Sh/Re_d^{1/2}$ for $z/d = 0.03$.

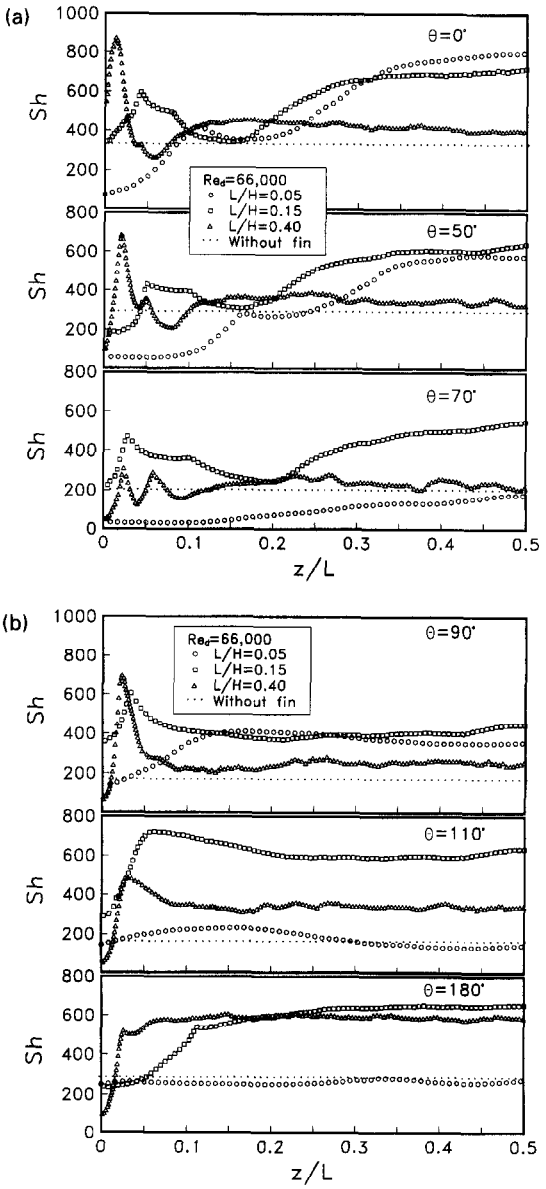

Fig. 11. (a) Variations of Sh along the cylinder for $Re_d = 66\,000$. $\theta = 0°$, 50° and 70°. (b) Variations of Sh along the cylinder for $Re_d = 66\,000$. $\theta = 90°$, 110° and 180°.

The objective was to depict the qualitative character of horseshoe vortices based on the mass transfer data in moderate Reynolds numbers $30\,000 \leqslant Re_d \leqslant 80\,000$, and over the ranges $0 \leqslant L/H \leqslant 0.40$. For a small gap distance ($L/H = 0.05$), most of sublimation takes place near the front region of the cylinder, especially around the separation region. The minimum value of Sh is moved slightly toward the front stagnation point ($\theta = 75°$). As the gap distance is moderate ($L/H = 0.15$), the mass transfer in the rear wake region is augmented. The influence of horseshoe vortices near the corner junction is significant and the overall character of horseshoe vortices shows a more organized pattern. The average mean mass transfer is twice larger than that of no fins. For a large gap distance ($L/H = 0.40$), the impact of horseshoe vor-

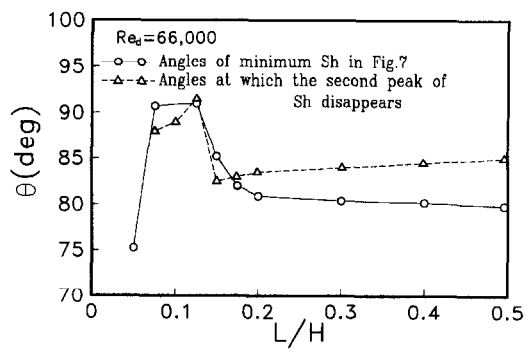

Fig. 12. Variations of the angle corresponding to minimum Sh and the angle of disappearing peak of Sh due to $V3$.

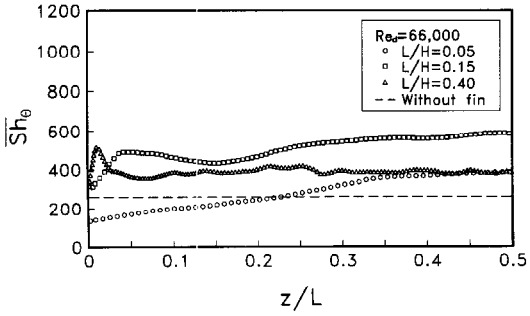

Fig. 13. Circumferential average *Sh* along the cylinder, $Re_d = 66\,000$.

tices on the corner junction in the vicinity of the endwall is substantial. As θ increases, the effect of vortex $V3$ becomes strong from the stagnation point before the separation, while the strength of vortex $V2$ is gradually attenuated. In the interior, the flow is seen to be nearly two-dimensional.

Acknowledgement—Appreciation is extended to the referees whose comments led to improvements of the paper.

REFERENCES

1. F. E. M. Saboya and E. M. Sparrow, Local and average transfer coefficients for one-row plate fin and tube heat exchanger configuration, *ASME J. Heat Transfer* **96,** 265–272 (1974).
2. R. A. Graziani, M. F. Blair, J. R. Taylor and R. E. Mayle, An experimental study of endwall and airfoil surface heat transfer in a large scale turbine blade cascade, *ASME J. Engng Power* **102,** 257–267 (1980).
3. P. A. Eibeck and J. K. Eaton, Heat transfer effects of a longitudinal vortex embedded in a turbulent boundary layer, *ASME J. Heat Transfer* **109,** 16–24 (1987).
4. P. T. Ireland and T. V. Jones, Detailed measurements of heat transfer on and around a pedestal in fully developed passage flow, *Proceedings of the 8th International Heat Transfer Conference*, San Francisco, CA, pp. 975–980 (1986).
5. E. M. Fisher and P. A. Eibeck, The influence of a horseshoe vortex on local convective heat transfer, *ASME J. Heat Transfer* **112,** 329–335 (1990).
6. H. J. Sung, M. S. Lyu and M. K. Chung, Local mass transfer from a circular cylinder in a uniform shear flow, *Int. J. Heat Mass Transfer* **34,** 59–67 (1991).
7. H. J. Sung, K. S. Hwang and J. M. Hyun, Experimental study on mass transfer from a circular cylinder in pulsating flow, *Int. J. Heat Mass Transfer* **37,** 2203–2210 (1994).
8. R. J. Goldstein and J. Karni, The effect of a wall boundary layer on local mass transfer from a cylinder in crossflow, *ASME J. Heat Transfer* **106,** 260–270 (1984).
9. W. A. Eckerle and L. S. Langston, Horseshoe vortex formation around a cylinder, *ASME J. Turbomach.* **109,** 278–285 (1987).
10. F. J. Pierce and M. D. Harsh, The mean flow structure around and within a turbulent junction or horseshoe vortex-part-II. The separated and junction vortex flow, *ASME J. Fluids Engng* **110,** 415–423 (1988).
11. F. J. Pierce and I. K. Tree, The mean flow structure on the symmetry plane of a turbulent junction vortex, *ASME J. Fluids Engng* **112,** 16–22 (1990).
12. N. Van Dreasar and R. E. Mayle, Convection at the base of a cylinder with horseshoe vortex, *Proceedings of the 8th International Heat Transfer Conference*, San Francisco, CA, pp. 1121–1126 (1986).
13. M. R. Visbal, Structure of laminar juncture flows, *AIAA J.* **29,** 1273–1282 (1991).
14. C. T. Baker, The laminar horseshoe vortex, part 2, *J. Fluid Mech.* **95,** 347–367 (1979).
15. L. S. Langston, M. L. Nice and R. M. Hooper, Three-dimensional flow within a turbine cascade passage, *ASME J. Engng Power* **99,** 21–28 (1977).
16. R. J. Goldstein, J. Karni and Y. Zhu, Effect of boundary conditions on mass transfer near the base of a cylinder in crossflow, *ASME J. Heat Transfer* **112,** 501–504 (1990).
17. E. M. Sparrow and S. R. Chastain, Effect of angle of attack on the heat transfer coefficient for an annular fin, *Int. J. Heat Mass Transfer* **29,** 1185–1191 (1986).
18. D. Ambrose, I. J. Lawrenson and C. H. S. Sparke, The vapor pressure of naphthalene, *J. Chem. Thermodyn.* **7,** 1173–1176 (1975).
19. N. H. Chen and D. F. Othmer, New generalized equation for gas diffusion coefficient, *J. Chem. Engng Data* **7,** 37–41 (1962).
20. A. Richter and E. Naudascher, Fluctuating on a rigid circular cylinder in confined flow, *J. Fluid Mech.* Part 3, **78,** 561–576 (1976).
21. T. Igarashi, Local heat transfer from a square frism to an airflow, *Int. J. Heat Mass Transfer* **29,** 777–784 (1986).